Effect of the observation length on the two-dimensional shadowing function of the sea surface: application on infrared 3–13-μm emissivity

Christophe Bourlier, Joseph Saillard, and Gérard Berginc

An analytical approach of the two-dimensional emissivity of a rough sea surface in the infrared band is presented. The emissivity characterizes the intrinsic radiation of the sea surface. Because the temperature measured by the infrared camera depends on the emissivity, the emissivity is a relevant parameter for retrieving the sea-surface temperature from remotely sensed radiometric measurements, such as from satellites. This theory is developed from the first-order geometrical-optics approximation and is based on recent research. The typical approach assumes that the slope in the upwind direction is greater than the slope in the crosswind direction, involving the use of a one-dimensional shadowing function with the observed surface assumed to be infinite. We introduce the two-dimensional shadowing function and the surface observation length parameters that are included in the modeling of the two-dimensional emissivity.

OCIS codes: 010.4450, 030.6600, 080.2720, 000.5490.

1. Introduction

The emissivity of a rough sea surface is an important parameter for correcting the surface temperature from radiometric sensors. It has been established that the surface temperature must be estimated to 0.1 K involving an emissivity error of approximately 0.002. Consequently the emissivity must be determined accurately. References 1–3 assume that the two-dimensional surface is isotropic and ignore the shadowing function. The model developed by Yoshimori *et al.*[4,5] is valid, because the average slopes of the sea surface are smaller than unity, allowing for the use of the one-dimensional Smith shadowing function. The theory is developed from the first-order geometrical-optics approximation, and multiple reflections are neglected. All cited references assume that the observed surface is infinite. In this paper the problem of the two-dimensional shadowing function and emissivity of the sea surface with respect to the observation length are investigated.

In Section 2 the two-dimensional shadowing function is calculated, and the one-dimensional case is studied to choose between the Wagner[6] or the Smith[7,8] shadowing function. The one-dimensional sea surface is generated for Gaussian and Lorentzian autocorrelation functions; the method applied is based on that expanded in Ref. 9. The effect of the observation length on the shadowing function is also compared with the correlation length given in Ref. 10. From the simulations it was established that Smith's formulation is the most suitable. A criterion was determined for comparing the effect of the observation length with the length correlation obtained from the height spatial autocorrelation function used in Ref. 10. The results obtained are generalized to the two-dimensional surface.

The emissivity is computed in Section 3 from the results obtained in Section 2 and the approach developed in Ref. 10. The emissivity then includes the wind direction, the incidence angle, the wind speed, and the observation length. The slope variance in the wind direction is estimated from the Cox and Munk capillary wave model,[11] whereas in Ref. 5 it is computed with Joint North Sea Wave Project (JONSWAP) gravity waves.

C. Bourlier (cbourlie@ireste.fr) and J. Saillard are with the Laboratoire Systèmes Electronique et Informatique/EP, Centre National de la Recherche Scientifique 2081, Ecole Polytechnique de L'Université de Nantes—Institut de Recherche de l'Enseignement Supérieur aux Techniques de l'Electronique, Rue Christian Pauc, La Chantrerie, BP 50609, 44306 Nantes Cedex 3, France. G. Berginc is with DS/DFO, Thomson-CSF Optronique, Rue Guynemer, BP 55, 78283 Guyancourt Cedex, France.

Received 18 October 1999; revised manuscript received 24 April 2000.

0003-6935/00/203433-10$15.00/0

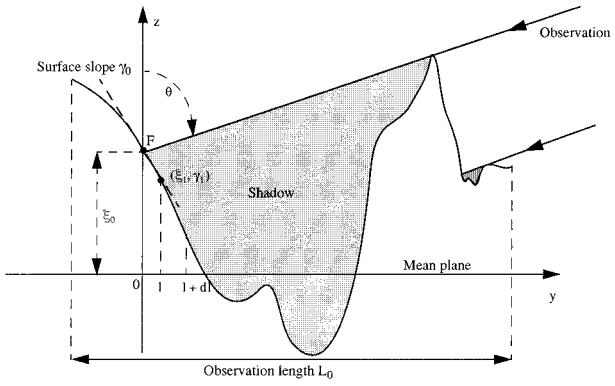

Fig. 1. Illustration of shadowing function.

In Section 4 the emissivity for an infinite surface is compared with that obtained in Ref. 5 and is simulated for different observation lengths. The values of the sea refraction index are given in Ref. 12.

2. Two-Dimensional Shadowing Function

The one-dimensional shadowing function is defined as the ratio of the illuminated surface. It varies between 0 for grazing incidence angles and 1 for normal incidence angles. In the literature the emissivity is either ignored[1–3] or computed by the approaches formulated by Wagner[6] or Smith.[7,8] The Smith shadowing function is similar to Wagner's, but Smith introduces a normalization function in the denominator. To compare these different models, the sea surface is generated with a Gaussian process, with Gaussian and Lorentzian autocorrelation functions. From the algorithm developed by Brokelman and Hagfors[9] and from the sea surface the exact solution of the shadowing function is then calculated. Since Smith and Wagner assume an infinite surface, the observation length effect on the shadow is studied, and the steps of the calculus of the one-dimensional shadowing function are presented to extend the results to the two-dimensional surface.

A. One-Dimensional Shadowing Function

1. Mathematical Development

For an observation length L_0 the shadowing function $S(\theta, F, L_0)$ is equal to the probability that the point $F(\xi_0, \gamma_0)$ on a random rough surface, of given height ξ_0 above the mean plane and with local slope $\gamma_0 = \partial z/\partial y$, is illuminated as the surface is crossed by an incident beam from incidence angle θ (Fig. 1),[6–8]

$$S(\theta, F, L_0) = \Upsilon(\mu - \gamma_0)\exp\left[-\int_0^{L_0} g(\theta|F; l)\mathrm{d}l\right], \quad (1)$$

with

$$\Upsilon(\mu - \gamma_0) = \begin{cases} 0 & \text{if } \gamma_0 \geq \mu \\ 1 & \text{if } \gamma_0 < \mu \end{cases}, \quad (1')$$

where $g(\theta|F; l)\mathrm{d}l$ is the conditional probability that the ray intersects the surface in the interval $[l; l + \mathrm{d}l]$ and with knowledge that the ray does not cross the surface in the interval $[0; l]$. Υ is the Heaviside function. In the Wagner (index W) and the Smith (index S) approaches, $g(\theta|F; l)\mathrm{d}l$ is defined as follows,

$$g_W(\theta|F; l) = \int_\mu^\infty (\gamma - \mu)p(\xi; \gamma|\xi_0, \gamma_0)\mathrm{d}\gamma, \qquad \xi = \xi_0 + \mu l,$$

$$g_S(\theta|F; l) = \frac{\displaystyle\int_\mu^\infty (\gamma - \mu)p(\xi; \gamma|\xi_0, \gamma_0)\mathrm{d}\gamma}{\displaystyle\int_{-\infty}^{\infty}\int_{-\infty}^{\xi_0+\mu l} p(\xi; \gamma|\xi_0, \gamma_0)\mathrm{d}\xi\mathrm{d}\gamma} = \frac{g_W(\theta|F; l)}{\displaystyle\int_{-\infty}^{\infty}\int_{-\infty}^{\xi_0+\mu l} p(\xi; \gamma|\xi_0, \gamma_0)\mathrm{d}\xi\mathrm{d}\gamma}, \quad (2)$$

where $p(\xi; \gamma|\xi_0, \gamma_0)$ is the slopes' $\{\gamma_0, \gamma\}$ and the heights' $\{\xi_0, \xi\}$ joint probability density and $\mu = \cot\theta$ is the slope of the incident ray. Note that Smith introduces a normalization function in the denominator.

The uncorrelated Gaussian process states that

$$p(\xi)p(\gamma) = \frac{1}{2\pi\sigma\omega}\exp\left(-\frac{\xi^2}{2\omega^2} - \frac{\gamma^2}{2\sigma^2}\right), \quad (3)$$

where $\{\omega^2, \sigma^2\}$ denote the height and the slope variances of the surface, respectively. When we substitute Eq. (3) into Eqs. (2), the integration over γ yields

$$g_W(l|F, \theta) = \mu\Lambda(v)\frac{1}{\omega\sqrt{2\pi}}\exp\left[-\left(\frac{\xi_0 + \mu l}{\sqrt{2}\omega}\right)^2\right],$$

$$g_S(l|F, \theta) = g_W(l|F, \theta)\frac{2}{1 + \mathrm{erf}\left(\dfrac{\xi_0 + \mu l}{\sqrt{2}\omega}\right)} \geq g_W(l|F, \theta), \quad (4)$$

with

$$\Lambda(v) = \frac{\exp(-v^2) - v\sqrt{\pi}\,\mathrm{erfc}(v)}{2v\sqrt{\pi}},$$

$$v = \frac{\mu}{\sqrt{2}\sigma} = \frac{\cot\theta}{\sqrt{2}\sigma}, \quad (4')$$

where {erf, erfc} denote the error and the complementary error functions, respectively. When we substi-

Table 1. Definition of the Autocorrelation Functions

	Gaussian	Lorentzian
Autocorrelation function	$\omega^2 \exp\left(-\frac{i^2}{L_c^{\,2}}\right)$	$\frac{\omega^2}{1+(i/L_c^{\,2})^2}$
Filter coefficient	$\omega\left(\frac{2}{L\sqrt{\pi}}\right)^{1/2}\exp\left(-\frac{2i^2}{L_c^{\,2}}\right)$	$2\omega\left(\frac{1}{L_c\pi}\right)^{1/2}\frac{1}{1+(2i/L_c)^2}$

tute Eqs. (4) into Eqs. (2), the integrations over l yields

$$S_W(\theta, F, L_0) = \Upsilon(\mu - \gamma_0)\exp\left\{-\frac{\Lambda}{2}\left[\operatorname{erfc}\left(\frac{\xi_0}{\sqrt{2}\omega}\right) - \operatorname{erfc}\left(\frac{\xi_0 + \mu L_0}{\sqrt{2}\omega}\right)\right]\right\},$$

$$S_S(\theta, F, L_0) = \Upsilon(\mu - \gamma_0)\left[\frac{1 - \frac{1}{2}\operatorname{erfc}\left(\frac{\xi_0}{\sqrt{2}\omega}\right)}{1 - \frac{1}{2}\operatorname{erfc}\left(\frac{\xi_0 + \mu L_0}{\sqrt{2}\omega}\right)}\right]^{\Lambda}. \quad (5)$$

Smith [Eq. (20) of Ref. 7] and Wagner [Eq. (17) of Ref. 6] assume an infinite surface $L_0 \to \infty$. The average shadowing function over the slopes γ_0 and the heights ξ_0 is defined as

$$S(\theta, L_0) = \int_{-\infty}^{\infty}\int_{-\infty}^{\infty} S(\theta, F\{\xi_0, \gamma_0\}, L_0)p(\xi_0, \gamma_0)\mathrm{d}\xi_0\,\mathrm{d}\gamma_0. \quad (6)$$

Substituting Eqs. (5) into Eq. (6), performing the integrations over the slopes γ_0 and the heights ξ_0, and using the variable transformation $h_0 = \xi_0/(\sqrt{2}\omega)$, for an uncorrelated Gaussian process we get

$$S_W(v, L_0) = \frac{1}{\sqrt{\pi}}\left[1 - \frac{1}{2}\operatorname{erfc}(v)\right]\int_{-\infty}^{\infty}\exp\left\{-h_0^{\,2} - \frac{\Lambda}{2}[\operatorname{erfc}(h_0) - \operatorname{erfc}(h_0 + y_0 v)]\right\}\mathrm{d}h_0,$$

$$S_S(v, L_0) = \frac{1}{\sqrt{\pi}}\left[1 - \frac{1}{2}\operatorname{erfc}(v)\right]\int_{-\infty}^{\infty}\exp(-h_0^{\,2}) \times \left[\frac{1 - \frac{1}{2}\operatorname{erfc}(h_0)}{1 - \frac{1}{2}\operatorname{erfc}(h_0 + y_0 v)}\right]^{\Lambda}\mathrm{d}h_0, \quad (7)$$

with

$$y_0 = \frac{L_0}{l_0}, \qquad l_0 = \frac{\omega}{\sigma}, \qquad v = \frac{\cot\theta}{\sqrt{2}\sigma}, \quad (7')$$

where y_0 is the normalized observation length with respect to the length l_0. The integration over h_0 is numerical, and for an infinite observation length this integration can be analytically determined [Eq. (24) of Ref. 7, Eq. (20) of Ref. 6]. The shadowing functions then depend on only one parameter, v.

2. Simulations

We compute the exact solution by generating the sampled surface $y(i)$, to compare the Smith and the Wagner shadowing functions. The method used is based on a Fourier transform.[13] Let $x(i)$ be the known sampled input signal, $y(i)$ the output signal to be determined, and $\{g(i), G(f)\}$ the spatial and frequency impulse response of the filter. The aim is to compute the filter coefficients, with knowledge of the autocorrelation function.

If $x(i)$ is a stationary random process of second order with a power spectral density $\Phi_x(f)$, then $y(i)$ is a stationary random second-order process, whose power spectral density $\Phi(f)$ verifies

$$\Phi(f) = |G(f)|^2\Phi_x(f). \quad (8)$$

Since the autocorrelation must be even, the impulse response is real, leading to

$$G(f) = [\Phi(f)/\Phi_x(f)]^{1/2}. \quad (9)$$

Furthermore,

$$y(i) = g(i) * x(i), \quad (10)$$

where $*$ is the convolution product. $y(i)$ is computed by application of Gaussian white noise with a variance $\omega_b{}^2$ to the input. Its power spectral density is equal to $\Phi_x(f) = \omega_b{}^2$. Substitution of Eq. (9) into Eq. (10) leads to

$$y(i) = (1/\omega_b)w(i) * x(i), \quad (11)$$

with

$$w(i) = TF^{-1}[\sqrt{\Phi(f)}]. \quad (11')$$

The filter coefficients for Gaussian and Lorentzian autocorrelation functions are given in Table 1. L_c denotes the length correlation, and the standard slope deviation σ is equal to the negative value of the autocorrelation function second derivative at 0. We obtain the numerical shadowing function by applying an algorithm defined in Ref. 9. In Fig. 2 the different shadowing functions [Eqs. (7) and numerical results] are plotted as functions of the parameter v for an infinite surface. We see that for grazing angles corresponding to $v \to 0$ the shadowing function tends

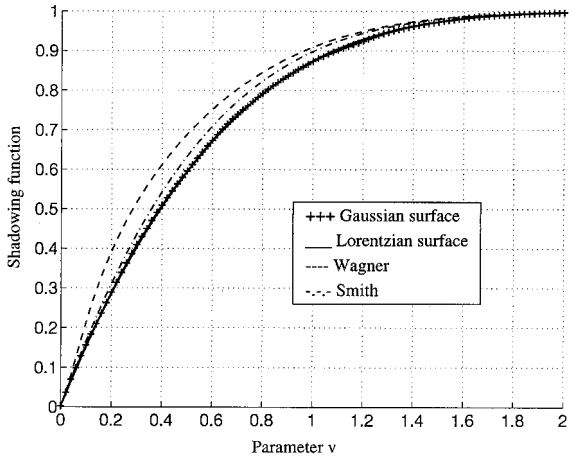

Fig. 2. One-dimensional shadowing function for an infinite surface as a function of the parameter v.

toward 0, whereas for normal angles $v \to 2$ it converges to 1, because the surface is entirely illuminated. In Fig. 3 the differences between the shadowing functions and the one defined for an infinite Gaussian surface are represented versus v. Since Wagner's difference is greater than Smith's, the Smith model is kept as comparison in this paper. It is also observed that the shadowing function for a Gaussian surface is similar to that obtained with a Lorentzian surface.

In Fig. 4 the one-dimensional Smith shadowing function is plotted as a function of v and y_0 [Eqs. (7)]. For v constant the shadowing function increases when y_0 decreases. In Fig. 5 the relative error between the one-dimensional Smith shadowing function and that obtained from an infinite surface is represented. It is defined in percentage by

$$E_S = 100 \times \frac{S_S(v, y_0) - S_S(v)}{S_S(v, y_0)}. \tag{12}$$

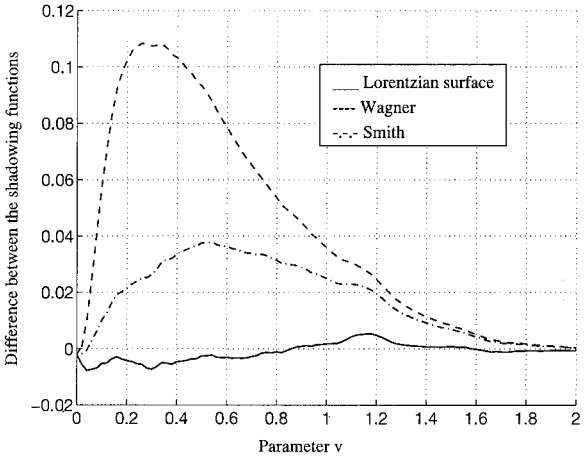

Fig. 3. Difference between one-dimensional shadowing functions for an infinite surface and that obtained from the infinite Gaussian surface.

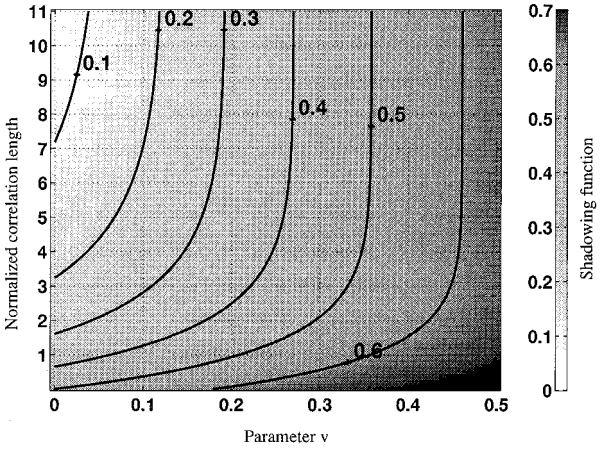

Fig. 4. Smith one-dimensional shadowing function as a function of parameter v and normalized correlation length.

The equation $y_0 = \sqrt{6}/v$ is plotted as a dashed curve. It is seen that this curve is similar to that obtained from a relative error equal to 0.1%. This means that the observation length can be assumed to be infinite, because $y_0 \geq \sqrt{6}/v$ is equivalent to $\theta \leq \theta_l = \text{atan}[L_0/(2\sigma\sqrt{3}l_0)]$ [Eqs. (7′)]. From the two-scale model[14] the parameter l_0 is computed with the gravity wave characterized by the height spatial autocorrelation function $R_0(l)$ defined as[10]

$$R_0(l) = \omega^2 \frac{\cos(l/L_c')}{1 + (l/L_c)^2}, \tag{13}$$

with

$$\omega^2 = 3.953 \times 10^{-5} u_{10}^{4.04}, \quad L_c = 0.154 u_{10}^{2.04}, \quad L_c' = 0.244 u_{10}^{1.91}; \tag{13'}$$

thus

$$l_0 = \frac{\omega}{\sigma} = \omega \Big/ \left(-\frac{\mathrm{d}^2 R_0}{\mathrm{d}l^2}\bigg|_{l=0} \right)^{1/2} = \frac{L_c}{[2 + (L_c/L_c')^2]^{1/2}}, \tag{14}$$

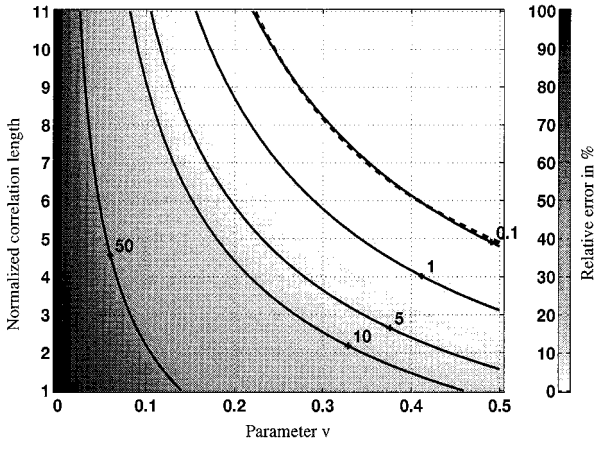

Fig. 5. Relative error between the Smith one-dimensional shadowing function and that obtained from an infinite surface.

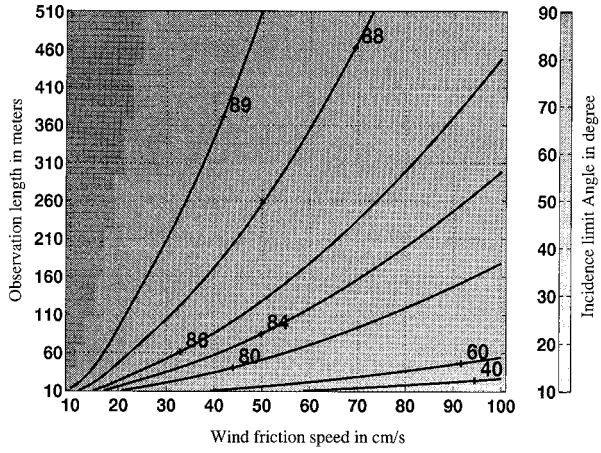

Fig. 6. Incidence limit angle as a function of wind friction speed and observation length.

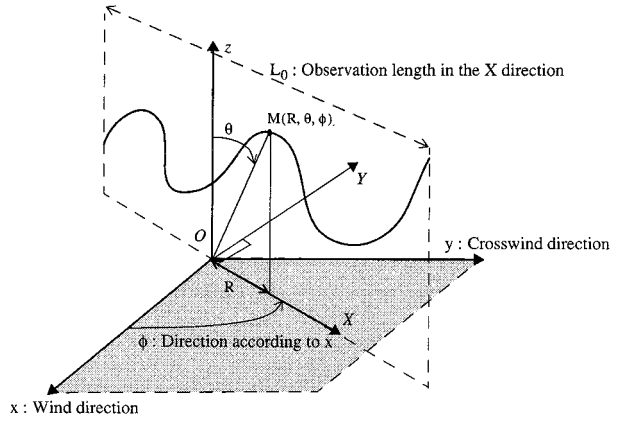

Fig. 7. Two-dimensional configuration of shadowing function.

where the slope variance σ^2 in the capillary wave is determined from the Cox and Munk model[11] given as

$$\sigma^2 = 0.003 + 5.08 \times 10^{-3} u_{12}, \tag{15}$$

where $\{u_{10}, u_{12}\}$ are the wind speeds at 10 and 12.5 m above sea level. The wind speed u_z, in centimeters/s, at an altitude z, in centimeters, is given as a function of the friction speed u_f, in centimeters/s, in[15]

$$u_z = \frac{u_f}{0.4} \ln\left(\frac{z}{z_0}\right), \tag{16}$$

with

$$z_0 = \frac{0.684}{u_f} + 4.28 \times 10^{-5} u_f^2 - 4.43 \times 10^{-2}. \tag{16'}$$

In Fig. 6 the limit angle θ_l is plotted with respect to the friction speed u_f, in centimeters/s, and the observation length L_0, in meters. As we show in Fig. 6, for a L_0 constant, θ_l decreases when u_f increases, whereas for a given u_f the limit angle is proportional to L_0. This means that for $\{u_f = 50$ cm/s; $L_0 = 260$ m$\}$ the surface can be considered to be infinite if the incidence angle is smaller than 88°.

B. Two-Dimensional Shadowing Function

In this subsection the one-dimensional shadowing function is extended to the two-dimensional sea surface. The two-dimensional shadowing function is characterized in polar coordinates by the azimuth angle ϕ (observation direction according to the wind) and by the incidence angle θ (Fig. 7). For a constant direction ϕ, the issue is one dimensional. The idea is to extend the one-dimensional results to the two-dimensional surface by execution of a rotation of an angle ϕ around the (Oz) axis. The one-dimensional joint probability density of the slopes and the heights becomes $p(\xi, \gamma_x, \gamma_y|\xi_0, \gamma_{0x}, \gamma_{0y}; x, y)$ in the wind (Ox) and the cross wind (Oy) directions. For an uncorrelated Gaussian surface the joint probability density is expressed in the (OX) (angle ϕ) direction as (see Appendix A)

$$p(\xi, \gamma_X) = \frac{1}{\omega \sigma_X 2\pi} \exp\left(-\frac{\gamma_X^2}{2\sigma_X^2} - \frac{\xi^2}{2\omega^2}\right), \tag{17}$$

with

$$\sigma_X^2 = \alpha + \beta \cos(2\phi), \quad \alpha = \frac{\sigma_x^2 + \sigma_y^2}{2},$$

$$\beta = \frac{\sigma_x^2 - \sigma_y^2}{2}, \tag{17'}$$

where σ_X^2 is the slope variance in the direction (OX) and $\{\sigma_x^2, \sigma_y^2\}$ are the slope variances in the upwind and the crosswind directions, respectively. When we compare Eqs. (17) and (3), the two-dimensional probability is obtained from the one-dimensional probability by substitution of

$$\begin{aligned} \gamma \quad & \text{with } \gamma_X, \\ \sigma \quad & \text{with } \sigma_X. \end{aligned} \tag{18}$$

Therefore from Eqs. (7) Smith's two-dimensional shadowing function is

$$S_S(\theta, \phi, L_0) = \frac{1}{\sqrt{\pi}} \left[1 - \frac{1}{2}\operatorname{erfc}(v)\right] \int_{-\infty}^{\infty} \exp(-h_0^2) \times \left[\frac{1 - 1/2 \operatorname{erfc}(h_0)}{1 - 1/2 \operatorname{erfc}(h_0 + y_0 v)}\right]^{\Lambda(v)} dh_0, \tag{19}$$

with

$$y_0(\phi) = \frac{L_0}{l_0(\phi)}, \qquad v = \frac{\cot\theta}{\sqrt{2}\sigma_X(\phi)}. \tag{19'}$$

In Figs. 8 and 9 Smith's two-dimensional shadowing function for an infinite observation length, and for $u_f = \{20, 40\}$ cm/s, is plotted as a function of the direction ϕ and the incidence angle θ. It is noted that the shadowing effect is important for angles close to 90°, that it decreases with wind speed, but that these results are hardly appreciable according to

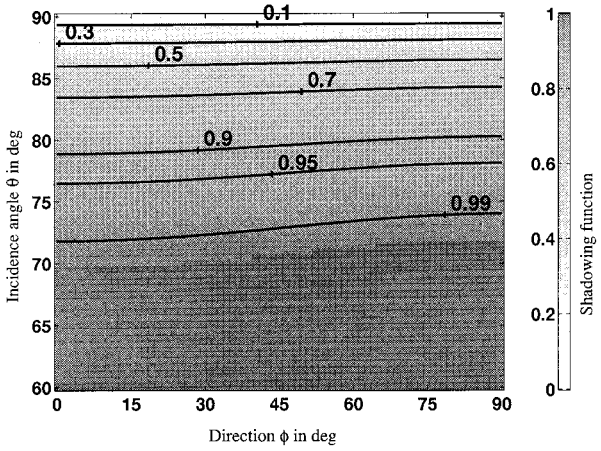

Fig. 8. Smith two-dimensional shadowing function for infinite observation length with $u_f = 20$ cm/s, function of direction ϕ, and incidence angle θ.

ϕ. The shadowing function then does not depend significantly on the anisotropy of the medium.

3. Application on the Two-Dimensional Emissivity

In this section the two-dimensional emissivity is determined. Yoshimori *et al.*[5] assumed that the slope in the upwind direction is greater than that defined in the crosswind direction, allowing for the use of a one-dimensional shadowing function. Our method includes the two-dimensional shadowing function established in Section 2. No hypothesis on the slope distribution is used, which is the original aspect of this paper, with reasoning based on Ref. 5.

A. Mathematical Development

Let M be a point of the surface defining the origin of Cartesian coordinates (x, y, z) (Fig. 10), $\mathbf{n}$ the unitary vector in the direction z, $\mathbf{n}'$ the unitary vector normal to the facet at M, and $\mathbf{s}$ the unitary vector of the

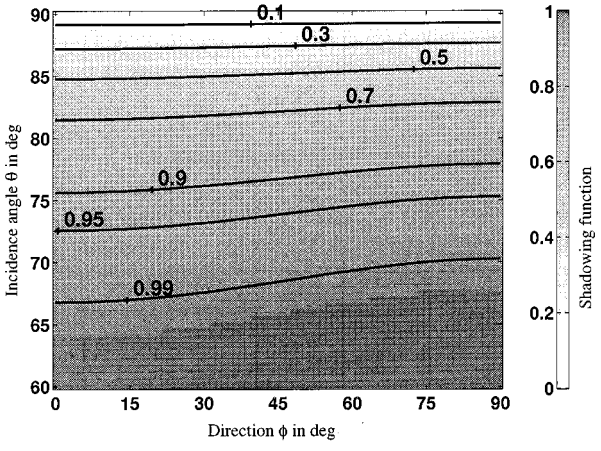

Fig. 9. Smith two-dimensional shadowing function for infinite observation length with $u_f = 40$ cm/s, function of the direction ϕ, and incidence angle θ.

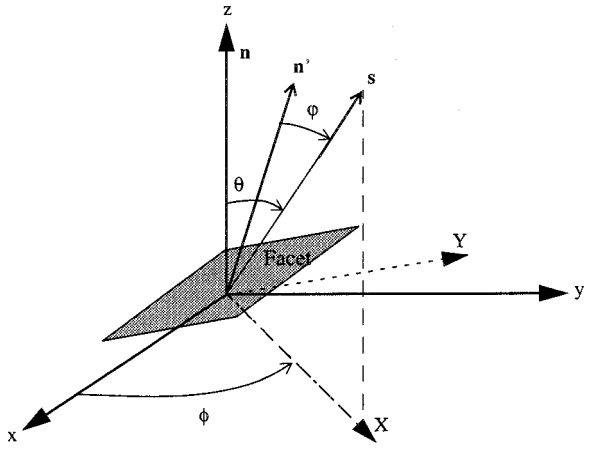

Fig. 10. Two-dimensional configuration of the facet.

viewing direction characterized by the $\{\theta, \phi\}$ angles. These vectors in polar coordinates are defined as

$$\mathbf{n} = \begin{pmatrix} 0 \\ 0 \\ 1 \end{pmatrix}, \quad \mathbf{n}' = \frac{1}{(1 + \gamma_x^2 + \gamma_y^2)^{1/2}} \begin{pmatrix} -\gamma_x \\ -\gamma_y \\ 1 \end{pmatrix},$$
$$\mathbf{s} = \begin{pmatrix} \sin\theta\cos\phi \\ \sin\theta\sin\phi \\ \cos\theta \end{pmatrix}, \tag{20}$$

where $\{\gamma_x, \gamma_y\}$ are the slopes of the surface in the wind and the crosswind directions.

Let $\varphi = (\mathbf{n}', \mathbf{s})$ be defined as follows:

$$\cos\varphi = \mathbf{n}' \cdot \mathbf{s} = \frac{\cos\theta - (\gamma_x \cos\phi + \gamma_y \sin\phi)\sin\theta}{(1 + \gamma_x^2 + \gamma_y^2)^{1/2}}. \tag{21}$$

If we assume that Kirchhoff's law [Eq. (9) of Ref. 3] is satisfied at the water–air interface, the local emissivity of the facet is expressed in the direction φ as

$$\epsilon = [1 - |r(|\varphi|)|^2], \tag{22}$$

where r is Fresnel's formula either in vertical polarization V (parallel to the incidence plane) or horizontal polarization (orthogonal to the incidence plane) given by

$$r_V(\varphi) = \frac{n\cos\varphi - \cos\varphi'}{n\cos\varphi + \cos\varphi'},$$
$$r_H(\varphi) = \frac{\cos\varphi - n\cos\varphi'}{\cos\varphi + n\cos\varphi'}, \qquad \text{with } \sin\varphi' = \sin\varphi/n, \tag{23}$$

where n is the refractive index of the sea water, φ is the incidence angle according to the normal facet, and φ' is the refraction angle that can be found by the Snell–Descartes law. The air refractive index is as-

sumed to be equal to 1. The slope anisotropy probability density $p(\gamma_x, \gamma_y)$ is assumed to be Gaussian,

$$p(\gamma_x, \gamma_y) = \frac{1}{2\pi(\sigma_x^2\sigma_y^2 - \sigma_{xy}^4)^{1/2}} \exp\left\{-\frac{1}{2}[y_x \quad \gamma_y] \times \begin{bmatrix} \sigma_x^2 & \sigma_{xy}^2 \\ \sigma_{xy}^2 & \sigma_y^2 \end{bmatrix}^{-1} \begin{pmatrix} \gamma_x \\ \gamma_y \end{pmatrix}\right\}, \quad (23')$$

where σ_{xy}^2 is the slope cross correlation.

For the two-dimensional autocorrelation function $R_0(x, y)$[10] to be even in the upwind (Ox) and crosswind the (Oy) directions, $\sigma_{xy}^2 = 0$, which leads to

$$p(\gamma_x, \gamma_y) = \frac{1}{2\pi\sigma_x\sigma_y} \exp\left(-\frac{\gamma_x^2}{2\sigma_x^2} - \frac{\gamma_y^2}{2\sigma_y^2}\right). \quad (23'')$$

References 1–3 assume that $\sigma_x^2 = \sigma_y^2 = \sigma^2$. When we introduce the shadowing function S, the average emissivity $\bar{\epsilon}$ for all facets of slopes $\{\gamma_x, \gamma_y\}$ is then equal to[5]

$$\bar{\epsilon}(\theta, \phi) = \frac{1}{2\pi\sigma_x\sigma_y} \int_{-\infty}^{\infty}\int_{-\infty}^{\infty} [1 - |r(|\varphi|)|^2] \exp\left(-\frac{\gamma_x^2}{2\sigma_x^2} - \frac{\gamma_y^2}{2\sigma_y^2}\right) \times g \times S \mathrm{d}\gamma_x \mathrm{d}\gamma_y, \quad (24)$$

where g is a normalization function defined in Ref. 5,

$$g = \frac{\mathbf{n}' \cdot \mathbf{s}}{(\mathbf{n} \cdot \mathbf{n}')(\mathbf{n} \cdot \mathbf{s})} = 1 - (\gamma_x \cos\phi + \gamma_y \sin\phi)\tan\theta. \quad (25)$$

Reference 5 neglects γ_y^2 in comparison with $1 + \gamma_y^2$, and Eqs. (21) and (25) become Eqs. (2.26) and (2.21), respectively, of Ref. 5, which is similar to assuming $\{\gamma_y, \phi\} = 0$. This means that the average emissivity is obtained from a single integration over γ_x. To use the two-dimensional shadowing function S, the emissivity has to be determined in the ϕ direction, i.e., in the new base (X, Y) as depicted in Fig. 10. From the previous coordinates (γ_x, γ_y) the new coordinates (γ_X, γ_Y) are

$$\gamma_x = \gamma_X \cos\phi - \gamma_Y \sin\phi,$$
$$\gamma_y = \gamma_X \sin\phi + \gamma_Y \cos\phi. \quad (26)$$

Substituting Eqs. (26) into Eqs. (24), we get

$$\bar{\epsilon}(\theta, \phi) = \frac{1}{2\pi(\alpha^2 - \beta^2)^{1/2}} \int_{-\infty}^{\infty}\int_{-\infty}^{\infty} [1 - |r(|\varphi|)|^2] \exp(-a\gamma_Y^2 - 2b\gamma_Y\gamma_X - c\gamma_X^2) \times g \times S \mathrm{d}\gamma_X \mathrm{d}\gamma_Y, \quad (27)$$

with

$$\cos\varphi = \frac{\cos\theta - \gamma_X \sin\theta}{(1 + \gamma_X^2 + \gamma_Y^2)^{1/2}} \qquad g = 1 - \gamma_X \tan\theta,$$
$$a = \frac{\alpha + \beta\cos(2\phi)}{2(\alpha^2 - \beta^2)}, \qquad b = \frac{\beta \sin(2\phi)}{2(\alpha^2 - \beta^2)},$$
$$c = \frac{\alpha - \beta\cos(2\phi)}{2(\alpha^2 - \beta^2)}, \qquad \alpha = (\sigma_x^2 + \sigma_y^2)/2,$$
$$\beta = (\sigma_x^2 - \sigma_y^2)/2. \quad (27')$$

Thus, for a finite observation length L_0, it is shown that the Smith average uncorrelated two-dimensional shadowing function [Eq. (19)] over the height is the following,

$$S_S(\theta, \phi, \gamma_X) = \frac{\Upsilon(\cot\theta - \gamma_X)}{\sqrt{\pi}} \int_{-\infty}^{\infty} \exp(-h_0^2) \times \left[\frac{1 - 1/2\ \mathrm{erfc}(h_0)}{1 - 1/2\ \mathrm{erfc}(h_0 + y_0 v)}\right]^{\Lambda(v)} \mathrm{d}h_0, \quad (28)$$

where $\{y_0(\phi), v\}$ are given by Eqs. (19′). Since the integration over γ_X is not computed, the term $1 - \mathrm{erfc}(v)/2$ is replaced with $\Upsilon(\cot\theta - \gamma_X)$. Substituting Eq. (28) into Eq. (27), we have

$$\bar{\epsilon}(\theta, \phi) = \frac{1}{2\pi\sqrt{\pi}(\alpha^2 - \beta^2)} \int_{-\infty}^{\infty} \left\{\int_{-\infty}^{\cot\theta} \times [1 - |r(|\varphi|)|^2] \exp(-a\gamma_Y^2 - 2b\gamma_Y\gamma_X - c\gamma_X^2) \times (1 - \gamma_X \tan\theta)\mathrm{d}\gamma_X\right\} \mathrm{d}\gamma_Y \int_{-\infty}^{\infty} \exp(-h_0^2) \times \left[\frac{1 - 1/2\ \mathrm{erfc}(h_0)}{1 - 1/2\ \mathrm{erfc}(h_0 + y_0 v)}\right]^{\Lambda(v)} \mathrm{d}h_0. \quad (29)$$

For an infinite observation length $y_0 \to \infty$, Eq. (29) becomes

$$\bar{\epsilon}(\theta, \phi) = \frac{1}{2\pi[\Lambda(v) + 1](\alpha^2 - \beta^2)^{1/2}} \times \int_{-\infty}^{\cot\theta} \exp(-c\gamma_X^2) \times (1 - \gamma_X \tan\theta)\left\{\int_{-\infty}^{\infty} [1 - |r(|\varphi|)|^2] \exp(-a\gamma_Y^2 - 2b\gamma_Y\gamma_X)\mathrm{d}\gamma_Y\right\} \mathrm{d}\gamma_Y. \quad (29')$$

Since the incidence angle θ is equal to 90°, i.e., $\{v, \mu\} \to 0$, Eq. (29′) leads to

$$\bar{\epsilon}(90°, \phi) = \frac{1}{\sigma_x[2\pi(\alpha^2 - \beta^2)]^{1/2}} \int_0^{\infty} \gamma_X \exp(-c\gamma_X^2) \left\{\int_{-\infty}^{\infty} \times [1 - |r(|\varphi|)|^2] \exp(-a\gamma_Y^2 - 2b\gamma_Y\gamma_X)\mathrm{d}\gamma_\gamma\right\} \mathrm{d}\gamma_X. \quad (29'')$$

Since in Ref. 3 the effect of the shadow is not taken into account, at grazing angles the mean emissivity diverges, because $\tan\theta$ tends to infinity. When the shadowing function is included, the quantity $\tan\theta/[\Lambda(v) + 1]$ converges to $\sqrt{2\pi}/\sigma_X$.

B. Simulations

In Fig. 11 the emissivities $[\bar{\epsilon}_V(\theta, \phi) + \bar{\epsilon}_H(\theta, \phi)]/2$ determined for $\phi = \{0°, 90°\}$ and $\theta = \{60°, 85°\}$ are compared with those obtained in Ref. 5, as a function of the wind speed u_{10} defined at 10 m above sea level. The refractive index of the water is equal to 1.19. There are two differences between the model in Ref. 5 and ours. No assumption is taken on the slope variance, whereas in Ref. 5 ${\gamma_y}^2$ is neglected in comparison with $1 + {\gamma_x}^2$. The second difference is the fact that Ref. 5 uses the slope variances obtained from the JONSWAP gravity spectrum, whereas in this paper the Cox and Munk capillary model is applied.

From the two-scale model,[14] the parameter l_0 is computed by use of the two-dimensional height spatial autocorrelation function $R_{2d}(l, \phi)$ defined[10] as

$$R_{2d}(1, \phi) = \omega^2 \left[\frac{R_0(l)}{\omega^2} - A \cos(2\phi) \frac{J_2\left(\frac{l}{L_2'}\right)}{1 + \left(\frac{l}{L_2}\right)^2} \right], \quad (30)$$

with

$$A = 3.439 \qquad L_2 = 0.157 u_{10}^{1.95} \qquad L_2' = 0.138 u_{10}^{2.05}; \quad (30')$$

thus

$$l_0(\phi) = \frac{\omega}{\sigma} = \frac{\omega}{\left\{ \frac{\partial^2}{\partial l^2} [-R_{2d}(l, \phi)] \Big|_{l=0} \right\}^{1/2}} = \frac{L_c}{[2 + (L_c/L_c')^2 + (A/4)\cos(2\phi)(L_c/L_2')^2]^{1/2}}, \quad (31)$$

with $\{{\sigma_x}^2, {\sigma_y}^2\}$ as the slope variances in the upwind and the crosswind directions determined from the Cox and Munk model[11] given by

$${\sigma_x}^2 = 3.16 \times 10^{-3} u_{12},$$
$${\sigma_y}^2 = 0.003 + 1.92 \times 10^{-3} u_{12}. \quad (31')$$

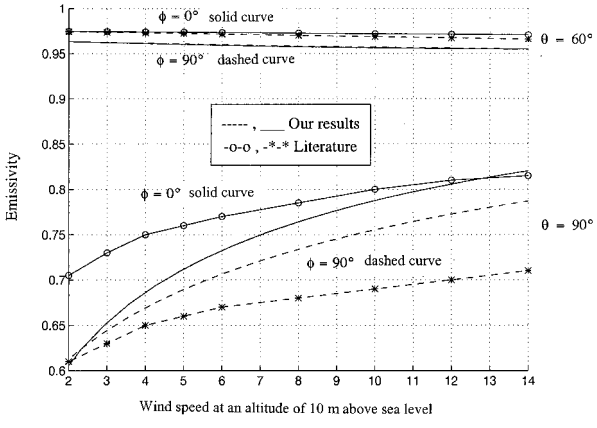

Fig. 11. Comparison of authors' results with those obtained in Ref. 5.

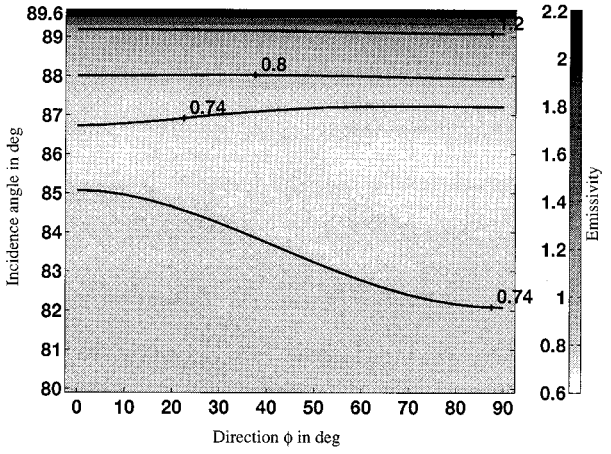

Fig. 12. Emissivity as a function of the direction ϕ and the incidence angle, for finite observation length of 60 m. $\{\lambda = 4\ \mu m, u_f = 40\ cm/s\}$.

The emissivity is plotted in Fig. 12 versus direction ϕ and the incidence angle θ for a finite observation length of 60 m. The wavelength $\lambda = 4\ \mu m$, and the friction speed $u_f = 40$ cm/s. The refractive index of the sea water $n(\lambda, T)$ is obtained from Ref. 12 with a temperature $T = 25$ °C. It is observed that the emissivity varies slightly with the direction ϕ, implying that the emissivity is weakly sensitive to the anisotropic factor of the sea surface. When the incidence angle is less than the limit angle θ_l, equal to 84° in Fig. 6, it is observed that the emissivity is similar to that calculated for an infinite observation length (Fig. 13), whereas for incidence angles much greater than 86° the emissivity increases, reaches 1 and finally converges to 2.2. This result has no physical meaning, because the emissivity must be lower than unity. The phenomenon occurs because the observation length y_0 in Eq. (29) is equal to a constant for any θ. In practice, when the incidence angle θ tends to 90°, the observation length becomes infinite, which means that the emissivity is similar to that obtained in Fig. 13 [Eq. (29′)]. The emissivity,

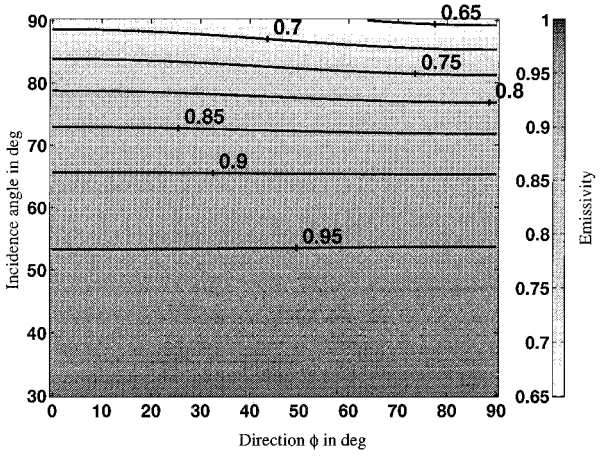

Fig. 13. Emissivity as a function of direction ϕ and incidence angle, for infinite observation length. $\{\lambda = 4\ \mu m, u_f = 40\ cm/s\}$.

with Wagner's shadowing function, was simulated, and a similar behavior is observed.

Note that the Wagner[6] and the Smith[7] one-dimensional shadowing functions assume that the slopes' $\{\gamma_0, \gamma\}$ and the heights' joint probability density is uncorrelated, which involves an overestimation of the shadow.[16] Moreover, Ricciardi and Sato[17,18] proved that the shadowing function is well defined by Rice's infinite series of integrals. The approach proposed then by Wagner retains only the first term of these series, whereas the Smith formulation uses the Wagner model and introduces a normalization function [Eqs. (2)].

4. Conclusion

The two-dimensional emissivity with respect to Smith's two-dimensional shadowing function has been investigated in this paper. It was calculated extensively for an uncorrelated Gaussian process and for a given observation length. Our model of the emissivity is based on Ref. 5, but contrary to this reference, no hypothesis on the slope behaviors of the sea surface is used. From simulations in the one-dimensional case the Smith shadowing function is chosen, because Smith's[7] results are close to the exact solution, whereas Wagner's[6] results are less accurate. A criterion for functions of the incidence angle and the wind speed is also found, which allows us to determine when the surface may be considered infinite. In the two-dimensional case, for an infinite surface, the simulations show that the emissivity decreases slightly with the wind direction and decreases with the incidence angle. For a constant finite observation length, we see that at grazing angles, i.e., when the criterion on an infinite surface is not verified, the emissivity is much greater than 1, which is not expected, because in practice the observation length increases with the incidence angle. Also, the Smith shadowing function model assumes that the heights' and the slopes' joint probability density is uncorrelated.[16]

Appendix A

The slopes' $\{\gamma_0, \gamma\}$ and the heights' $\{\xi_0, \xi\}$ one-dimensional joint probability density $p(\xi; \gamma|\xi_0, \gamma_0)$ becomes $p(\xi, \gamma_x, \gamma_y|\xi_0, \gamma_{0x}, \gamma_{0y}; x, y)$ in the directions $\{(Ox), (Oy)\}$, so for an uncorrelated Gaussian process,

$$p(\xi, \gamma_x, \gamma_y) = \frac{1}{\sqrt{2\pi}^3 \sqrt{|[C^{xy}]|}} \exp(-1/2\mathbf{V}^{\mathbf{xy}T}[C^{xy}]^{-1}\mathbf{V}^{\mathbf{xy}}), \tag{A1}$$

with

$$[C^{xy}] = \begin{bmatrix} \omega^2 & 0 & 0 \\ 0 & \sigma_x{}^2 & 0 \\ 0 & 0 & \sigma_y{}^2 \end{bmatrix}, \qquad \mathbf{V}^{\mathbf{xy}} = \begin{pmatrix} \xi \\ \gamma_x \\ \gamma_y \end{pmatrix}, \tag{A2}$$

where $\{\sigma_x{}^2, \sigma_y{}^2\}$ are the slope variances in the upwind and the crosswind directions, respectively, and ω^2 is the height variance. The exponent xy denotes the base (x, y), and the symbol T is the transpose vector. Since the correlation is not included, the probability is independent of the height spatial autocorrelation function. To determine the slope probability density $p(\xi, \gamma_x, \gamma_y)$ in the direction ϕ, we use a base transformation (X, Y, z). The former coordinates (γ_x, γ_y) are expressed in the new form (γ_X, γ_Y) as

$$\mathbf{V}^{\mathbf{xy}} = \begin{pmatrix} \xi \\ \gamma_x \\ \gamma_y \end{pmatrix} = \begin{bmatrix} 1 & 0 & 0 \\ 0 & \cos\phi & -\sin\phi \\ 0 & \sin\phi & \cos\phi \end{bmatrix} \begin{pmatrix} \xi \\ \gamma_X \\ \gamma_Y \end{pmatrix} = [O_3]\mathbf{V}^{\mathbf{XY}}. \tag{A3}$$

Thus

$$\mathbf{V}^{\mathbf{xy}T}[C^{xy}]^{-1}\mathbf{V}^{\mathbf{xy}} = \mathbf{V}^{\mathbf{XY}T}([O_3]^{-1}[C^{xy}][O_3])^{-1}\mathbf{V}^{\mathbf{XY}}, \tag{A4}$$

with $[O_3]^T = [O_3]^{-1}$. When we substitute Eqs. (A2) and (A3) into Eq. (A4), and use Eq. (A1), the probability density $p(\xi, \gamma_x, \gamma_y)$ in the base (x, y) becomes $p(\xi, \gamma_X, \gamma_Y)$ in the base (X, Y) (Jacobian factor equal to 1),

$$p(\xi, \gamma_X, \gamma_Y) = \frac{1}{\sqrt{2\pi}^3 \omega\sigma_X\sigma_Y(1-\rho^2)^{1/2}} \exp\left[-\frac{\xi^2}{2\omega^2} - \frac{1}{2(1-\rho^2)}\left(\frac{\gamma_X{}^2}{\sigma_X{}^2} + \frac{\gamma_Y{}^2}{\sigma_Y{}^2} - \frac{2\rho\gamma_X\gamma_Y}{\sigma_X\sigma_Y}\right)\right], \tag{A5}$$

with

$$\begin{aligned} \sigma_X{}^2 &= \alpha + \beta\cos(2\phi), \\ \sigma_Y{}^2 &= \alpha - \beta\cos(2\phi), \\ \rho &= \frac{-\beta\sin(2\phi)}{\{\alpha^2 - [\beta\cos(2\phi)]^2\}^{1/2}}, \end{aligned} \tag{A6}$$

where $\alpha = (\sigma_x{}^2 + \sigma_y{}^2)/2$, $\beta = (\sigma_x{}^2 - \sigma_y{}^2)/2$; $\{\sigma_X{}^2, \sigma_Y{}^2\}$ are the slope variances in ϕ and $\phi + \pi/2$ directions; and ρ is the slope cross-correlation coefficient. The probability in the direction ϕ is obtained by calculation of the marginal probability $p(\xi, \gamma_X)$ defined as

$$p(\xi, \gamma_X) = \int_{-\infty}^{\infty} p(\xi, \gamma_X, \gamma_Y)\mathrm{d}\gamma_Y, \tag{A7}$$

which leads to

$$p(\xi, \gamma_X) = \frac{1}{\omega\sigma_X 2\pi} \exp\left(-\frac{\gamma_X{}^2}{2\sigma_X{}^2} - \frac{\xi^2}{2\omega^2}\right). \tag{A8}$$

References

1. K. Masuda, T. Takashima, and Y. Takayama, "Emissivity of pure and sea waters for the model sea surface in the infrared window regions," Remote Sens. Environ. **24,** 313–329 (1988).
2. P. M. Saunders, "Shadowing on the ocean and the existence of the horizon," J. Geophys. Res. **72,** 4643–4649 (1967).
3. X. Wu and W. L. Smith, "Emissivity of rough sea surface for 8–13 mm: modeling and verification," Appl. Opt. **36,** 2609–2619 (1997).
4. K. Yoshimori, K. Itoh, and Y. Ichioka, "Thermal radiative and

reflective characteristics of a wind-roughened water surface," J. Opt. Soc. Am. **11,** 1886–1893 (1994).
5. K. Yoshimori, K. Itoh, and Y. Ichioka, "Optical characteristics of a wind-roughened water surface: a two-dimensional theory," Appl. Opt. **34,** 6236–6247 (1995).
6. R. J. Wagner, "Shadowing of randomly rough surfaces," J. Opt. Soc. Am. **41,** 138–147 (1966).
7. B. G. Smith, "Lunar surface roughness, shadowing and thermal emission," J. Geophys. Res. **72,** 4059–4067 (1967).
8. B. G. Smith, "Geometrical shadowing of a random rough surface," IEEE Trans. Antennas Propag. **AP-5,** 668–671 (1967).
9. R. A. Brokelman and T. Hagfors, "Note of the effect of shadowing on the backscattering of waves from a random rough surface," IEEE Trans. Antennas Propag. **AP-14,** 621–627 (1967).
10. C. Bourlier, J. Saillard, and G. Berginc, "Spatial autocorrelation function of the heights of an even sea spectrum," presented at Poster Sessions (Phenomenology), 5th International Conference on Radar Systems, La Société des Electriciens et des Electroniciens, 17–21 May 1999, Brest, France.
11. C. Cox and W. Munk, "Statistics of the sea surface derived from sun glitter," J. Mar. Res. **13,** 198–226 (1954).
12. G. M. Hale and M. R. Querry, "Optical constants of water in the 200-nm to 200-μm wavelength region," Appl. Opt. **12,** 555–563 (1973).
13. M. Kunt, *Traitement de l'information VI: techniques modernes de traitement numériques des signaux* (Presses Polytechniques Romandes, France, 1991).
14. F. Daout, "Etude de la dépolarisation des ondes centimétiques par une surface rugueuse—Application au domaine maritime," Thèse de Doctorat (Institut de Recherche de l'Enseignement Supérieur aux Techniques de l'Electronique, Nantes, France, 1996).
15. H. L. Chan and A. K. Fung, "A theory of sea scatter at large incident angles," J. Geophys. Res. **82,** 3439–3444 (1977).
16. C. Bourlier, J. Saillard, and G. Berginc, "Effect of correlation between shadowing and shadowed points on the Wagner and Smith monostatic one-dimensional shadowing functions," IEEE Trans. Antennas Propag. **48,** 437–446 (2000).
17. L. M. Ricciardi and S. Sato, "On the evaluation of first passage time densities for Gaussian processes," Signal Process. **11,** 339–357 (1986).
18. L. M. Ricciardi and S. Sato, "A note on first passage time problems for Gaussian processes and varying boundaries," IEEE Trans. Inf. Theory **IT-29,** 454–457 (1983).